Crystal structure of archaeal IF5A-DHS complex reveals insights into the hypusination mechanism

Mattia D'Agostino[1,2], Angelita Simonetti[2], Stefano Motta[3], Philippe Wolff[2], Alice Romagnoli[1,4], Astra Piccinini[1], Francesco Spinozzi[1], Daniele Di Marino[1,4,5*], Anna La Teana[1,4*], Eric Ennifar[2*]

1 Department of Life and Environmental Sciences, Polytechnic University of Marche, Via Brecce Bianche, 60131 Ancona, Italy.

2 Architecture et Réactivité de l'ARN, CNRS UPR 9002, Institut de Biologie Moléculaire et Cellulaire, Université de Strasbourg, Strasbourg, France.

3 Department of Earth and Environmental Sciences, University of Milano Bicocca, Piazza della Scienza 1, 20126 Milan, Italy.

4 New York-Marche Structural Biology Center (Ny-Masbic), Polytechnic University of Marche, Via Brecce Bianche, 60131 Ancona, Italy.

5 Neuronal Death and Neuroprotection Unit, Department of Neuroscience, Mario Negri Institute for Pharmacological Research-IRCCS, Via Mario Negri 2, 20156 Milano, Italy.

*Corresponding author.

E-mail: e.ennifar@unistra.fr, d.dimarino@univpm.it, a.lateana@univpm.it

SUMMARY

The translation factor IF5A is a highly conserved protein in Eukarya and Archaea carrying a unique post-translational hypusine modification. Hypusination of IF5A requires the Deoxyhypusine Synthase (DHS) enzyme which transfers the butylamine moiety from spermidine to IF5A using NAD as a cofactor, forming a deoxyhypusine intermediate. IF5A is a key player in protein synthesis, preventing ribosome stalling in proline-rich sequences during translation elongation and facilitating translation elongation and termination. Additionally, human eIF5A has been shown to be involved in various essential cellular processes and its overexpression in cancer drives migration and metastasis, while inhibiting hypusination exerts anti-proliferative effects. The hypusination pathway of IF5A is therefore an attractive new therapeutic target. To this end, we have solved the 2.0 Å X-ray crystal structure of the archeal DHS-IF5A complex, revealing a hetero-octameric architecture and providing a detailed view of the complex active site including the hypusination loop. This structure, along with biophysical data and molecular dynamics simulations, provides new insights into the catalytic mechanism of the hypusination reaction.

Keywords: X-ray structure, oncogenesis, deoxyhypusine synthase, Initiation Factor 5A

INTRODUCTION

Hypusination is a post-translational modification that occurs exclusively to the translation initiation factor 5A (IF5A). The reaction is carried out by two enzymes: Deoxyhypusine Synthase (DHS or DHPS) and Deoxyhypusine Hydroxylase (DOHH). While the DHS catalyzes the production of a deoxyhypusine (N-(4-aminobutyl) lysine) intermediate by transferring the butylamine moiety from spermidine to a specific lysine residue of IF5A, using nicotinamide adenine dinucleotide (NAD) as cofactor (Joe et al., 1997; Wolff et al., 1997), DOHH hydroxylates the deoxyhypusine giving rise to the hypusinated form of IF5A (Park and Wolff, 2018).

IF5A is an evolutionary conserved protein, shared by Eukarya and Archaea, which plays a crucial role in the process of protein synthesis. It exerts its main function during translation elongation by facilitating peptide bond formation thus avoiding ribosome stalling (Dever et al., 2014; Gutierrez et al., 2013; Pelechano and Alepuz, 2017), but it has also been implicated in translation initiation and termination (Manjunath et al., 2019; Mathews and Hershey, 2015). In addition to its role as a translation factor, it has been suggested to play a role in other processes such as RNA binding, RNA turnover, nucleocytoplasmic transport, and even RNA degradation in the case of the archaeal protein. Hypusination is a prerequisite for most of these activities (Bassani et al., 2018; Hoque et al., 2017; Romagnoli et al., 2022; Schrader et al., 2006; Valentini et al., 2002; Wagner and Klug, 2007; Xu et al., 2004; Zuk, 1998).

Human IF5A exists in two isoforms, eIF5A1 and eIF5A2 both of which undergo hypusination. They show distinct cell-specific patterns of expression and have been implicated in many key cellular processes like

ageing, mitochondrial metabolism, autophagy, but also in several pathological conditions like diabetes, viral infection and propagation, neurodevelopmental disorders, and different types of cancer. The roles of the two isoforms in all these processes have been described and reviewed (Barba-Aliaga and Alepuz, 2022; Kulkarni et al., 2022; Park et al., 2022; Sfakianos et al., 2022; Tauc et al., 2021). Overexpression of both isoforms has been detected in several types of cancer and was shown to trigger cell migration, invasion and metastasis (Nakanishi and Cleveland, 2016). In particular, eIF5A2 is considered a potential oncogene as well as a diagnostic and prognostic marker in several malignancies such as ovarian, gastric and bladder cancer (Nakanishi and Cleveland, 2016). Furthermore, reducing the levels of eIF5A and DHS or inhibiting the hypusination reaction has been demonstrated to exert a potent anti-proliferative effect, leading to cell growth arrest and apoptosis (Nakanishi and Cleveland, 2016; Ning et al., 2020; Wu et al., 2020).

Based on these findings, the hypusination pathway is nowadays considered a significant and promising therapeutic target. Various compounds that inhibit both enzymes involved in the hypusination reaction have been characterized (Nakanishi and Cleveland, 2016; Turpaev, 2018). Among these compounds, N1-guanyl-1,7-diamineheptane (GC7) has been identified as the most effective inhibitor of DHS, while Ciclopirox has been found to be effective against DOHH activity. Unfortunately, most of these compounds show several drawbacks like scarce selectivity or adverse side effects (Turpaev, 2018). Therefore, designing new, more effective, and more specific compounds capable of inhibiting hypusination and overcoming these defects would be of fundamental importance. The design of new inhibitors can be boosted by a detailed knowledge of the three-

dimensional organization of the three proteins and of the complexes they form during the reaction.

The 3D structure of the single proteins, from different organisms, has been known for many years (Liao et al., 1998; Umland et al., 2004; Wątor et al., 2020), while the structure of a complex between eIF5A and a K329A mutant DHS has only recently been solved by cryoelectron microscopy (cryoEM) at 2.8 Å resolution (Wątor et al., 2023). This structure reveals only a single eIF5A molecule interacting with all four active sites of DHS tetramer, involving the hypusination loop of eIF5A and inducing subtle conformational changes in DHS. The latter study provides first insights into the structural basis of the interaction between DHS and eIF5A and clarifies the contribution of single residues involved in the interaction, shedding light on the effect of DHS mutations related to neurodegenerative disorders. However, it was obtained under spermidine-saturated conditions with eIF5 in substoichiometry amounts, leaving open the question of the biologically relevant eIF5/DHS stoichiometry.

Here we report the X-ray structure of the archaeal IF5A-DHS (aIF5A-aDHS) complex at 2.0 Å resolution showing four aIF5A molecules bound to aDHS tetramer core, as well as biophysical data supporting the observed stoichiometry. In addition, we have used molecular dynamic simulation to analyze the binding mode of spermidine, shedding light on the catalytic mechanism of the hypusination reaction. Overall, our findings provide novel insights into the molecular basis of this crucial post-translational modification and may contribute to the development of new therapeutic strategies targeting the hypusination pathway.

RESULTS AND DISCUSSION

Architecture of the aIF5A-aDHS complex

Recombinant aDHS and aIF5A (Supplementary Fig. 1) were used to solve the X-ray structure of the aIF5A-aDHS complex at 2.0 Å resolution (Supplementary Table 1), showing a highly compact aDHS tetramer bound to four aIF5A. Each aIF5A binds one aDHS monomer, thus forming a turtle-like structure where the aDHS tetramer would be the shell and aIF5As as limbs (Fig. 1a). In agreement with already available DHS structures (Liao et al., 1998; Umland et al., 2004; Wątor et al., 2020), the *S. islandicus* DHS is a homotetramer, with two tightly associated dimers per asymmetric unit (Fig. 1b, Supplementary Fig. 2a). Therefore, the enzyme can be considered as a dimer of dimers (A1-B1, B2-A2 on Fig. 1) with two distinct active sites at each dimer's interface that are composed by residues belonging from each of the two monomers (Fig. 1b). This structural organization of DHS has been reported as the active form of this enzyme (Liao et al., 1998). The core of each monomer contains a Rossman fold (Supplementary Fig. 2a), typical of most dehydrogenases and binds NAD, a cofactor of aIF5A hypusination and copurified with the enzyme. As previously described, the aDHS N-terminal end has a structural motif called "ball-and-chain" in which the first N-terminal 35 residues constitute the chain, while two α-helix turns (α1, Asn3-Lys9) form the ball (Liao et al., 1998). Interestingly, this structural motif is positioned just below the aDHS active site which is so free to receive and bind aIF5A.

aIF5A is made of two domains linked by an inter-boundary loop (Fig. 1c, Supplementary Fig. 2b) (Tong et al., 2009). While the C-terminal domain of the four *S. solfataricus* aIF5A and the hinge are mostly floppy and ill-defined due to the lack of crystal contacts, the N-terminal domain

interacting with aDHS is clearly visible in electron density maps, including the hypusine loop enclosing the lysine 36 (Lys36) which undergoes hypusination by the aDHS enzyme (Fig. 2a). This suggests that, even in absence of the spermidine substrate, it is properly structured to expose the Lys36 for hypusination in the context of the aDHS-aIF5A complex.

In the aDHS active site, NAD is bound at the A_1/B_1 and A_2/B_2 dimers interface (Fig. 2b,c). In both dimers, the aDHS active site forms a cavity established by four helices, α13 and α14 from one monomer and α9 and α12 from a second monomer. The N-terminal domain of each aIF5A binds the tetramer by leaning on dimers interfaces (Fig. 1a, Fig. 3a and Fig. 3b), forming a buried area of 548 $Å^2$ and 490 $Å^2$ with each monomer (Supplementary Fig. 3). Thus, the N-terminal domain of aIF5A allocates its antiparallel β_2 sheet comprising the hypusine loop within the cleft formed at the aDHS dimer interface, thereby exposing the $_{aIF5A}$Lys36 for aDHS-guided hypusination in the narrow tunnel of the enzyme active sites (Fig. 3b and Fig. 3c). In this structure, $_{aIF5A}$Lys36 points toward key residues for the hypusination reaction such as $_{aDHS}$His244, $_{aDHS}$Trp283 and $_{aDHS}$Lys285 (Fig. 3c).

The modification of lysine $_{aIF5A}$Lys36 into deoxyhypusine occurs with the participation of a spermidine and of a NAD molecules, substrate and cofactor of the reaction, which also bind within the active site of DHS. The internal cavity of aDHS active site is accessible through a 24 Å long tunnel that narrows at the site of interaction between the NAD nicotinamide ring and the sidechain of $_{aDHS}$Lys288. As the tunnel is formed in between the two monomers of the aDHS's dimer, the NAD molecules bound in the active site of each aDHS's dimer are very close to each other, being located at 3.0 Å between the two O3' atoms that establish a

hydrogen bond. The two nucleoside moieties of the NAD molecule form nine hydrogen bonds with residues belonging to one aDHS monomer, while only three hydrogen bonds are formed with the second aDHS monomer through the NAD phosphate groups. (Fig. 3d).

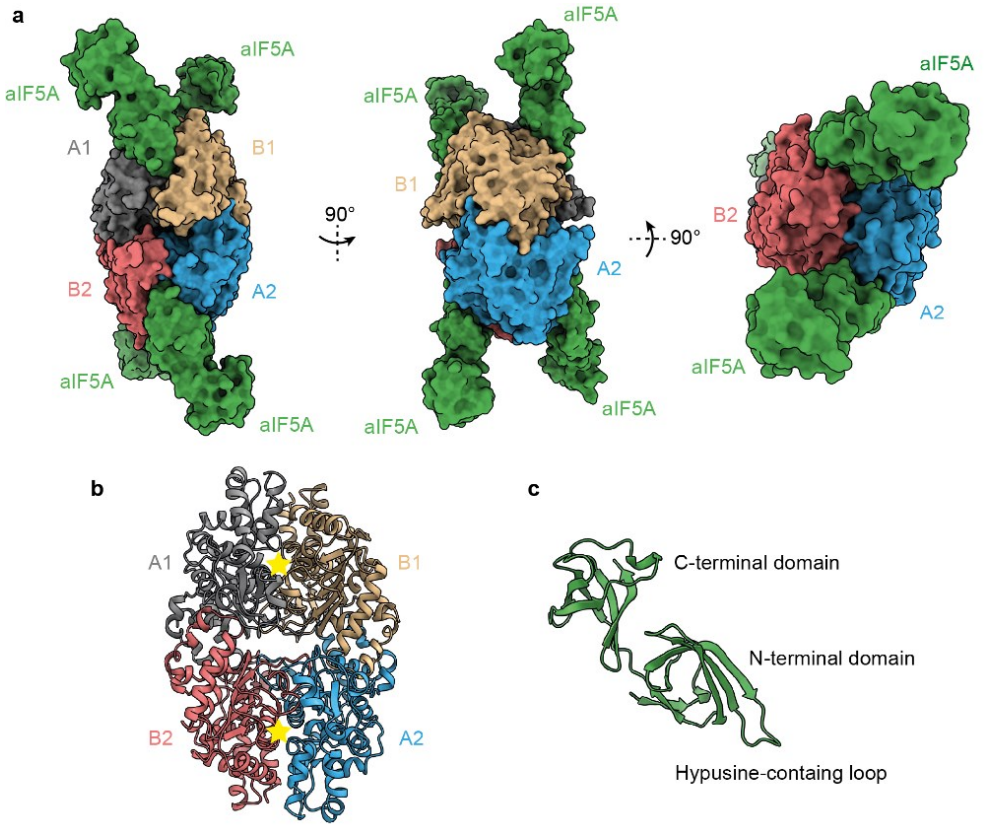

Fig. 1 | The overall structure of aIF5A-aDHS complex. (**a**) **a**IF5A-aDHS complex is shown as surface representation in three distinct orientations (front, side and bottom view). aIF5A and individual aDHS monomers are differently colored and labeled. (**b**) Front view of the aDHS tetramer represented as ribbon with yellow stars indicating the location of the active sites at each dimer interface. (**c**) Front view of aIF5A represented as ribbon; the location of the hypusine-containing loop, N-terminal domain and C-terminal domain are indicated. For **b** and **c** the color scheme is the same reported in **a**.

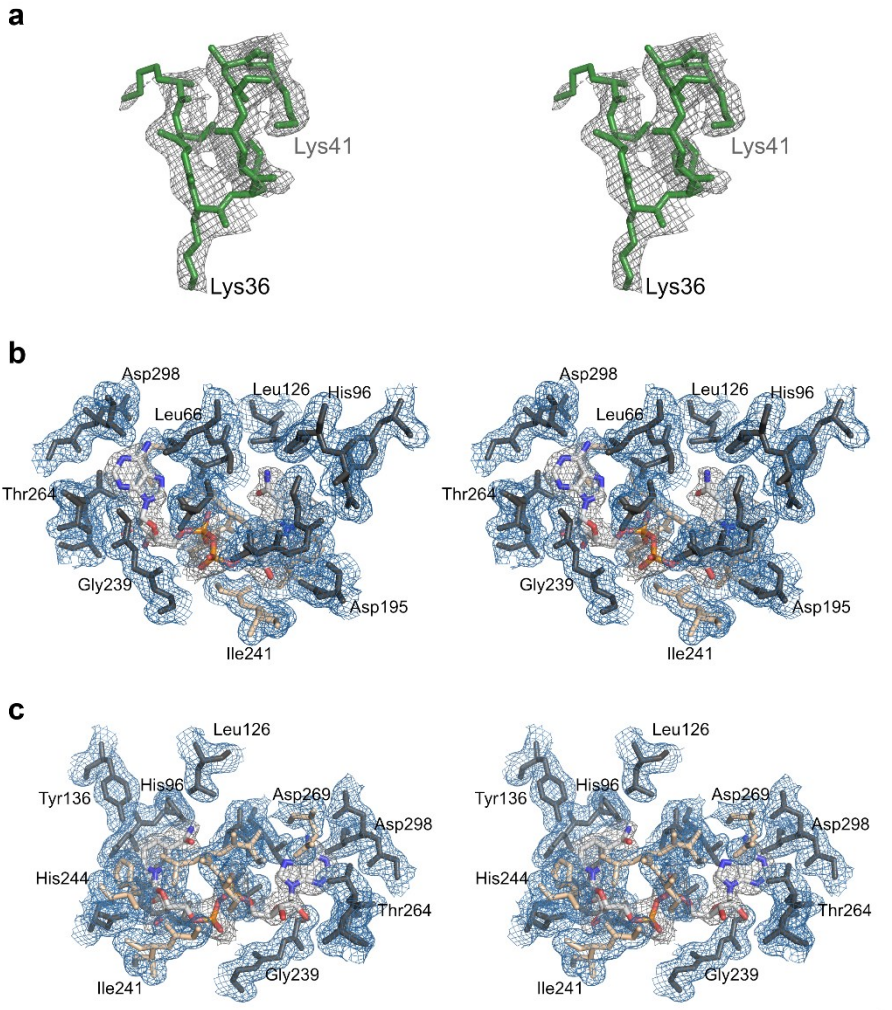

Fig 2. | Crossed-eyes stereo view of the aIF5A hypusine loop and the NAD binding pocket of aDHS. (**a**) The 2Fo-Fc electron density map contoured at 1.2σ level is shown around residues 33 to 41 of aIF5A. (**b-c**) Different views of the 2Fo-Fc electron density map contoured at 1.2 σ level is shown in grey around NAD and in blue around residues of monomers A1 (in dark grey) and B1 (in beige) of aDHS.

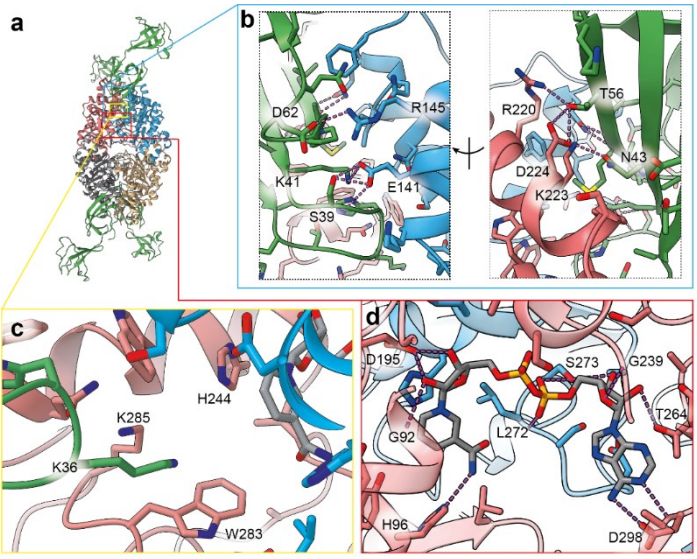

Fig 3. | aIF5A and NAD interacting with aDHS. (**a**) Ribbon representation of aIF5A-aDHS complex used to indicate: (**b**) the interaction interface between aDHS and aIF5A; (**c**) hypusination site $_{aIF5a}$Lys36 within the aDHS active site; (**d**) the interaction between one NAD molecule and two aDHS monomers inside the active site. Key residues are shown as sticks. For all panels, the color scheme is the same reported in Fig. 1. The dashed lines represent H-bonds.

Comparison of the X-ray structure with human complex

The recent resolution of the human complex structure (Wątor et al., 2023) has enabled us to make a direct comparison with it, in order to verify the conservation of the interaction, as well as the individual structure of the two proteins (Fig. 4a,b,c). The two complexes exhibit a different stoichiometry, with only one eIF5A molecule bound to the DHS tetramer in the human complex (Wątor et al., 2023), compared to archaea, which instead presents four molecules of aIF5A bound to a single tetramer. From a structural perspective, the archaeal complex remarkably fits the human structure, including the aIF5A-aDHS interaction, the hypusine loop

conformation, and the NAD binding site in the active site (r.m.s.d. = 0.97 Å between 221 atom pairs) (Fig. 4a,b,c), however with some significant differences located in the external parts of the DHS tetramer. Archaeal and human DHS and IF5A sequences and structures were also compared separately. Using amino acid alignment with the program M-COFFEE (Wallace, 2006) (Supplementary Fig. 4 and Supplementary Fig. 5), sequence identity and similarity were found to be 28.1% and 47.6 % for DHS and 26.3% and 46.7 % for aIF5A, respectively. Regarding IF5A, the overall root mean square deviation (RMSD) is 1.9 Å for 91 aa; The N-terminal domain contains the majority of conserved sequences, with an identity and similarity of 35.7% and 54.3%, and an RMSD of 0.7 Å for 50 amino acids when compared to its human counterpart (PDB ID 3CPF) (Tong et al., 2009); the C-terminal domain, on the other hand, is less conserved. Moreover, the alpha-helix found in some Eukaryal organisms, including humans, is absent in the C-terminal domain (Fig. 4d). The residues composing the hypusination loop (Gly35-Lys36-His37-Gly38), ordered in the present aIF5A-aDHS complex structure, are strictly conserved in the human protein (Gly49-Lys50-His51-Gly52) (Supplementary Fig. 4), but were not observed in the human eIF5A X-ray structure due to a lack of crystal contacts (Tong et al., 2009).

Superposition of *S. islandicus* DHS with *H. sapiens* DHS (PDB ID 6XXH) (Wątor et al., 2020) showed both structures are highly comparable (Fig. 4e; Supplementary Fig. 6, Supplementary Fig. 7 and Supplementary Fig. 8), with an RMSD of 1.0 Å for 229 aa. Although *S. islandicus* and *H. sapiens* DHS have similar overall structures, a significant difference is located in the Pro76-Thr95 region, where in human enzyme a two-turn alpha-helix (composed of Ser78-Asn86 residues) is found but not present

in the *S. islandicus* DHS (Fig. 4e). This extra region is highly flexible and superposition with some of the *H. sapiens* structures shows that this helix may collide with the interacting aIF5A in the present complex (Fig. 4e). Moreover, the previously described "ball and chain" domain (Liao et al., 1998; Umland et al., 2004; Wątor et al., 2020), which blocks the entrance to the active site in *H. sapiens* DHS (Liao et al., 1998) and allows the active site to be free in subsequently reported structures (Umland et al., 2004; Wątor et al., 2020), is also present in the aDHS structure (Asn3-Gly35). It is positioned just below the active sites, allowing aIF5A to bind the enzyme freely.

According to previous structural and biochemical analyses (Lee et al., 2001) the key residues within the DHS active site for hypusination reaction in humans are His288 (proton donor/acceptor), Trp327 and Lys329 (directly binding the butyloamine moiety from Spermidine). In *S. islandicus* DHS, counterpart residues such as $_{aDHS}$His244, $_{aDHS}$Trp283, and $_{aDHS}$Lys285 are conserved, highlighting the importance of these residues for hypusine formation. However, only $_{aDHS}$His244 is well-defined in electron density maps, while $_{aDHS}$Trp283 and $_{aDHS}$Lys285 are likely floppy in absence of the Spermidine substrate. In the DHS-IF5A interface, the sequence alignment (Supplementary Fig. 4 and Supplementary Fig. 5) has shown an identity of 28% and 40 % for DHS and aIF5A residues respectively involved in the mutual interaction. Concerning the binding with NAD and Spermidine, the overall DHS residues involved in the interaction are mostly conserved in human with an identity of 58.8% and 62.5 %, respectively (Supplementary Fig. 5).

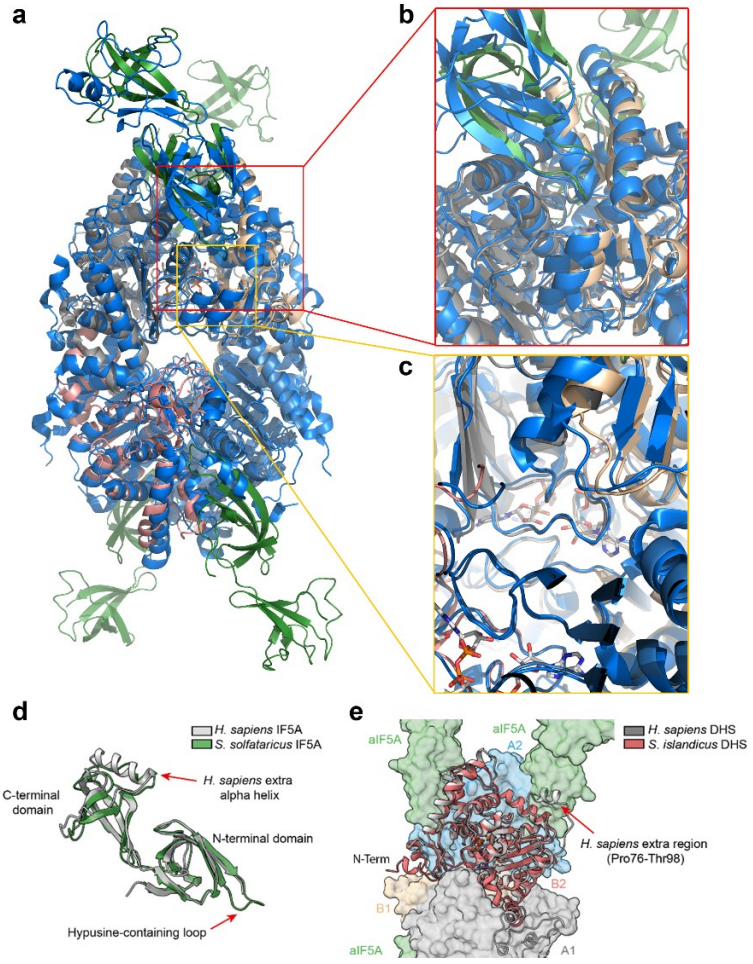

Fig 4. | Archaeal and Human IF5A-DHS complex are structurally conserved. (**a**) Superposition of the archaeal complex (same color code as Fig. 1) and the human one (PDB ID 8A0E, in dark blue). (**b**) Close-up of the aIF5A hypusine loop interacting with aDHS in the archaeal complex (same color code as Fig. 1) crystal structure and human DHS (PDB ID 8A0E, in dark blue) CryoEM structure. (**c**) Close-up of the DHS tetramer catalytic core showing the remarkable agreement between the aDHS (same color code as Fig. 1) crystal structure and human DHS (PDB ID 8A0E, in dark blue) CryoEM structure. Differences are restricted to the external regions of the tetramer. (**d**) Superposition of *S. solfataricus* IF5A (green) with *H. sapiens* IF5A (silver); C-terminal domain, N-terminal domain, Hypusine-containing loop and *H. sapiens* C-terminal extra alpha-helix are shown and labeled. (**e**) Superposition of one *S. islandicus* DHS monomer (red) with *H. sapiens* DHS monomer (silver). The other components of the complex are reported as surface representation and labeled to better understand the spatial organization. *H. sapiens* extra region is indicated by a red arrow.

Recently, Ganapathi et al. identified rare variants in DHS associated with decreased enzyme activity and reduced eIF5A hypusination (Ganapathi et al., 2019). To investigate whether the archaeal complex could be used as a model for studying this condition (DHS deficiency), we compared the corresponding residues in the human (Asn173, Tyr305, and Ile306) to those in *S. islandicus* ($_{aDHS}$Phe133-$_{aDHS}$Tyr261-$_{aDHS}$Val262). Notably, Tyr261 and Val262 are conserved in the archaeal complex, given that Ile and Val are both nonpolar amino acids (Supplementary Fig. 5). Furthermore, Phe133 is located at entrance of the active site, while Tyr261 and Val262 are situated within the chamber where the reaction takes place, explaining why hypusination is impaired in these cases. Taken together, these elements, when comparing the human complex to the archaeal complex of aIF5A-DHS, strongly suggest that the latter can be considered a reliable model for its human counterpart and is valuable for the design of novel hypusination inhibitors.

Biophysical and computational analyses of the aDHS-aIF5A binding

Considering the different stoichiometry of IF5A between human cryoEM complex and archaeal X-ray structure, we used Isothermal Titration Calorimetry (ITC) to gain insights into the stoichiometry and thermodynamics of the aIF5A binding to aDHS. ITC is a true label-free and in-solution technique providing the complete thermodynamic profile of a binding interaction, including ΔH, ΔS, ΔG, K_a and reaction stoichiometry. It reveals the forces driving complex formation and provides insights into complex formation. It is a perfectly complementary approach to structural approaches that only offer a final snapshot of the complex. ITC data at 30°C show that the aDHS-aIF5A interaction is

exothermic and strongly enthalpy-driven at this temperature (Fig. 5a), with a binding affinity in the low micromolar range (Table 1). Data were collected also at lower temperatures (25°C, 20°C and 5°C, Table 1, Supplementary Fig. 9a) to evaluate the temperature-dependance of the binding parameters and assess the heat capacity change ΔC_p of the binding reaction (Fig. 5b). At 5°C, the interaction turns endothermic and is entropy-driven due to a markedly negative heat capacity change of -635 $cal.mol^{-1}.K^{-1}$., which is the hallmark of local folding coupled to binding (Spolar and Record, 1994). Based on these data, the analysis of the number of folded residues following binding yields an estimation of $\mathfrak{R}^{th} \simeq 32$ residues for the entire aIF5A-aDHS complex. This estimation, purely based on thermodynamic basis, is remarkably coherent with the observation in the crystal structure of the eight residues Lys33 to Ala40 of the four aIF5A hypusine loop that are flexible in the free protein (Tong et al., 2009), but become structured when bound to the aDHS tetramer. The kinetics of the aIF5A binding to aDHS were also investigated using kinITC, an approach that obtains both kinetic and thermodynamic parameters, providing on- and off-rates as robustly as surface plasmon resonance approaches (Burnouf et al., 2012). The kinITC analysis of data at 30°C yields $k_{(on)} = (6.5 \pm 2.5) \times 10^3\ M^{-1}.s^{-1}$ and $k_{(off)} = (1.74 \pm 0.07) \times 10^{-2}\ s^{-1}$ (Supplementary Fig. 9b), indicating a rapid association between partners and suggesting that the complex forms quickly, with a moderate off-rate.

The ITC data also shows that the stoichiometric ratio between aDHS and aIF5A is close to 1.0, in agreement with the complex observed in the crystal structure. The presence of complexes with a 4:4 stoichiometry was further assessed in more diluted solution by native mass

spectrometry (Supplementary Fig. 10) and synchrotron SEC-SAXS analysis (SAXS results are discussed in Supplementary Data, Supplementary Fig.11,12,13). To investigate whether varying the number of bound aIF5A molecules could lead to significant changes in the structure and dynamics of the complex, we performed extensive molecular dynamics (MD) simulations using various stoichiometric composition of the complex (Supplementary Fig. 14). The overall stability of the complex was assessed by computing the root mean square fluctuations (RMSF) on the aDHS chains (Supplementary Fig. 15a). No significative difference was found in presence or absence of interactions with aIF5A and the structural elements that form the fold of aDHS displayed low fluctuations in all the simulations. The overall stability of the complexes was also confirmed by the unaltered radius of gyration of the complex (Supplementary Fig. 15b). The analysis of the aIF5A N-terminal domain RMSD and the aDHS-aIF5A number of contacts revealed that the dynamic behavior of the complex at the protein-protein interface is not significantly altered by the binding of a different number of aIF5A chains (Supplementary Fig. 14b,c). This was also confirmed by the monitor of the variation of Solvent Accessible Surface Area (ΔSASA) that measure the extension of the aDHS:aIF5A binding interface (Supplementary Fig. 15c).

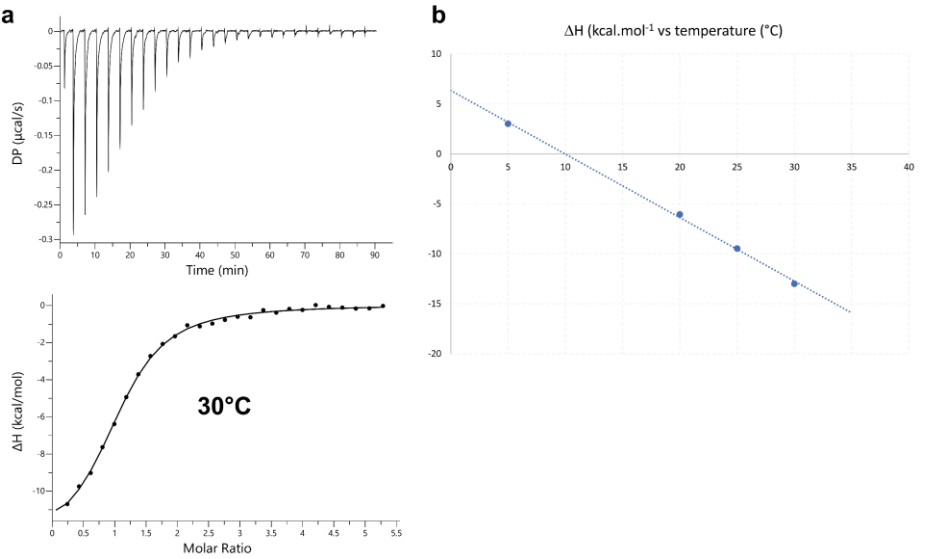

Fig. 5 | Thermodynamic analysis of the aIF5A/DHS complex (**a**) ITC thermogram for aIF5A binding to aDHS at 30°C. (**b**) The temperature-dependence of ΔH following complex formation. ΔCp is given by the slope of the linear fit. ITC data collection was not feasible at 10°C and 15°C due to the anticipated ΔH values at these temperatures being too low. Fitting of the temperature dependance of binding enthalpy with a linear regression yields ΔCp=-363 cal.mol^{-1}.K^{-1}. Fitting of the temperature dependance of binding entropy with a linear regression yields Ts=295.5 K, where Ts is the temperature where ΔS(T)=0.

Table 1. Summary of ITC data collected on the aDHS-aIF5A complex.

Temperature (°C)	ΔH (kcal.mol^{-1})	-TΔS (kcal.mol^{-1})	ΔG (kcal.mol^{-1})	Kd (µM)	N
5	3.0 ± 0.2	-11.1	-8.0	0.48 ± 0.15	0.91 ± 0.01
20	-6.1 ± 0.3	-2.1	-8.1	0.96 ± 0.19	1.04 ± 0.01
25	-9.5 ± 0.2	1.3	-8.2	1.1 ± 0.1	1.07 ± 0.01
30	-13.0 ± 0.3	5.3	-7.8	2.5 ± 0.2	1.06 ± 0.01

Specifically, the N-terminal domains of aIF5A exhibit fluctuations around the crystallographic position, resulting in RMSD values ranging from 6 to 7Å. However, these fluctuations do not impact the stability of the interaction with aDHS. To further investigate whether these fluctuations

differ when varying the number of bound aIF5A molecules, we also conducted principal component (PC) analysis of aIF5A motion for the aggregated simulated systems. The first two PCs describe the domain fluctuation of aIF5A, which is more pronounced in the C-terminal domain, located on the opposite side of the aDHS binding region. Upon comparing the sampled region in the PC1 and PC2 subspace, it can be noted that the behavior of all the simulated systems is similar (Supplementary Fig. 14d). These analyses confirmed that binding of additional aIF5A chains does not significantly affect the already bound chains.

Spermidine binding mode

Subsequently, we examined the interaction between spermidine and the aDHS-aIF5A complex, as we hypothesized that this polyamine could directly impact the enzyme's binding to aIF5A. To investigate the binding mechanism, we conducted molecular docking calculations of spermidine using the Glide software. All the standard docking attempts, however, failed to produce a pose within the aDHS binding site, probably due to the steric hindrance of some protein sidechains. For this reason, we attempt an induced fit docking (IFD) protocol that allows flexibility in the active-site sidechains. Surprisingly, even though we allowed flexibility in all the binding site sidechains and made only minor adjustments to a few protein sidechains during this procedure, the resulting docking pose was similar to the one observed in human DHS (hDHS) (PDB ID 6XXJ). In this way, the resulting binding pose displayed some key features common to the hDHS-spermidine complex. In particular, spermidine forms anchoring interactions at both ends: on one side an H-bond with S197, a salt bridge with D95, and a pi-cation interaction with W248; on the other

side a salt bridge with E279 and an H-bond with the NAD molecule (Fig. 6a). Moreover, additional H-bonds with K285 and H244 stabilize the central part of the molecule. Interestingly, this became possible thanks to few side chains conformational changes: the shift of the $_{aIF5A}$K36 towards the outside of the binding site, a rotation of $_{aDHS}$K285 to form an interaction with spermidine, a small adjustment of W248 to enlarge cavity and to form a pi-cation interaction and, finally, the rotation of the bulky W283 sidechain (Fig. 6b). All the other residues were not changed significantly by the IFD calculation. It is interesting to note that the role of the flexibility of the W283 sidechain was largely discussed in the recent hDHS cryo-EM structure (W327 in hDHS) (Wątor et al., 2023) and appears to be relevant also for the spermidine binding in aDHS. Indeed, we want to underline that W283 and most of the residues that moves to accommodate spermidine in aDHS present a weak electron density in the X-ray structure, that can be interpreted as high flexibility that allows adaptation to the substrate. It is interesting to point out how organisms far in evolution preserved the same binding mode features (anchors at the opposite ends of the substrate and few H-bonds in the middle) despite relevant changes in the residues that compose the binding site (Fig. 6c,d).

Finally, we investigated the possibility of accounting for receptor flexibility through an ensemble docking approach. To this end, we performed standard docking on structures sampled during MD simulations (details in Method section). These calculations did not produce any pose with reasonable RMSD (lower than 2.5 Å) from the human structure (Supplementary Table 2). On the contrary, the IFD protocol on some of the structures of the ensemble provided good poses (RMSD = 1.2Å), that are in line with the one described above. These results suggest a strong

induced fit effect of the spermidine substrate on the aDHS binding site. Furthermore, the binding between aDHS and aIF5A, or aDHS and spermidine, cannot coexist, highlighting the sequential nature of the deoxyhypusine reaction rather than a concurrent process.

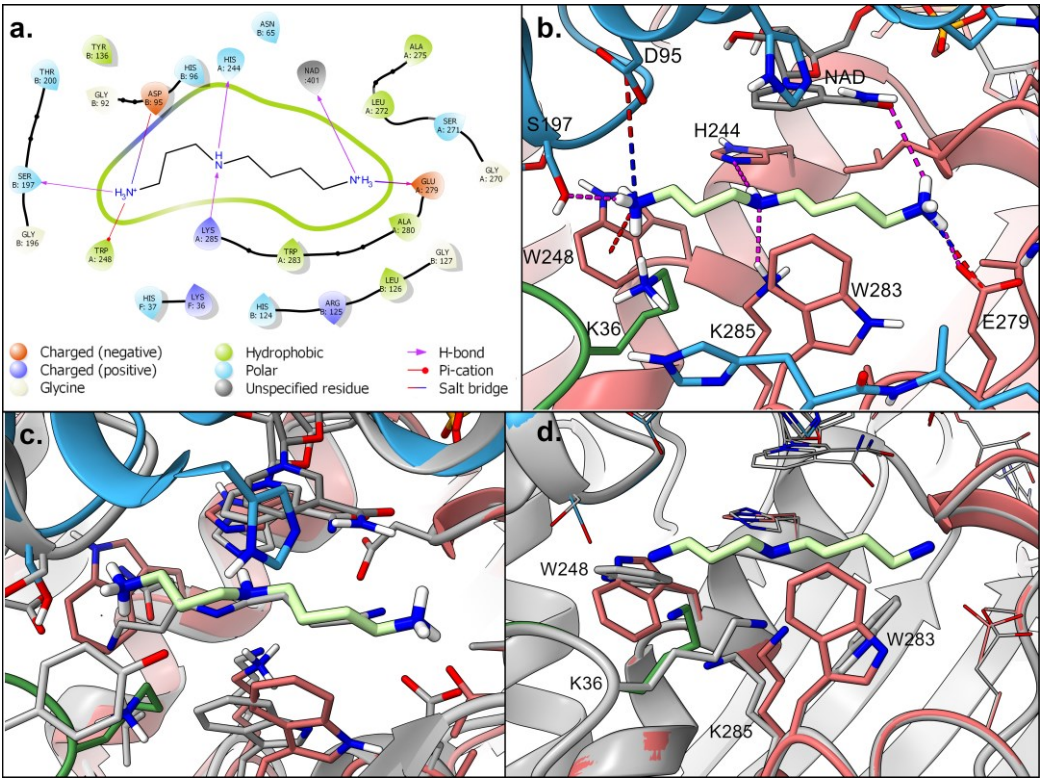

Fig. 6 | Spermidine Induced Fit Docking pose in aDHS. (**a**) 2D ligand interaction diagram showing all residues within 5 Å from the ligand; (**b**) 3D representation of the binding pose. Interactions are shown in dashed lines (H-bonds in magenta; salt-bridges in red/blue pi-cation in red. (**c**) Comparison of spermidine binding mode in aDHS (colored sticks) and hDHS (grey sticks). (**d**) Comparison of aDHS binding site before and after the Induced Fit Docking of Spermidine. Residues as resolved in the X-ray structure are shown in grey, while after the Induced Fit Docking of Spermidine colored according to their chain (aDHS light-blue and salmon, aIF5A in green). Residues that undergo substantial conformational changes are represented as bold sticks and labelled.

CONCLUSIONS AND PERSPECTIVES

Although the deoxyhypusine synthesis reaction between DHS and IF5A has been extensively studied from a biochemical and structural point of view over the years, several aspects are still not fully understood. Here, we present the first high-resolution crystallographic structure of the aDHS-aIF5A complex from an archaeon and thoroughly characterize its thermodynamics, kinetics, and stoichiometry. The complex is formed by four aIF5A molecules and a single aDHS tetramer. Each aIF5A molecule binds at the dimeric interface of the enzyme and interacts with the active site almost exclusively through the hypusination loop, resembling a lock-and-key mechanism.

Recently, the CryoEM structure of a human DHS-eIF5A complex was reported (Wątor et al., 2023). This complex exhibits high similarities and striking differences with the archaeal complex from this study. The most prominent difference lies in the 1:4 stoichiometry observed in the eIF5E-DHS cryoEM structure, as opposed to the 4:4 stoichiometry in the present aIF5A-aDHS X-ray structure. Native mass spectrometry, ITC calorimetry, as well as SAXS analysis reported here clearly show that the 4:4 archaeal complex is formed in solution and cannot result from a crystal packing artefact. Consequently, we wondered whether the different molecular compositions of the complex between human and archaeal complexes could somehow influence its stability or induce conformational changes. To address these questions, we subjected the various possible complexes to extensive molecular dynamics analysis, reaching the conclusion that each composition (including 1:4 and 3:4 stoichiometries) is stable and conformationally unchanged. Several factors in the experimental setup for CryoEM sample preparation may have influenced the eIF5A stoichiometry

in the human complex: (i) the presence of a large excess of spermidine, (ii) the use of a two-fold molar excess of eIF5A vs DHS only, and (iii) the use of a DHS mutant on the amino acid acceptor of the 4-aminobutyl group (DHS^{K329A}) by the polyamine mentioned above. Consequently, spermidine is "trapped" in the enzyme's active site, unable to fulfil its role and hindering the subsequent binding with eIF5A, as demonstrated by our docking studies and Wator's findings (Wątor et al., 2023). In the present aIF5A-aDHS complex, the wild-type enzyme was used and the complete absence of spermidine in the experimental setup allows to achieve the observed 4:4 aIF5A-aDHS stoichiometry. Apart from this difference in stoichiometry, the two complexes show remarkable structural similarities, especially in the DHS active site and NAD binding pocket, underlining the high similarity between the human and archaeal complexes.

In conclusion, our study, suggests that within a cell, the donation of the 4-aminobutyl group by spermidine and its acceptance by IF5A is a highly dynamic process. Indeed, it occurs rapidly, sequentially, and continuously, ensuring the availability of the hypusinated protein to the cell. Noteworthy, considering the high conservation between the human and archaeal proteins, the present high-resolution structure of the aIF5A-aDHS complex is a valuable model for structure-based drug design.

MATERIALS AND METHODS

For crystallization of the DHS-IF5A complex, we used proteins from different yet closely related organisms that maintain their respective proteins. *S. solfataricus* aIF5A shows a 97.7% identity with the corresponding protein in *S. islandicus*, differing only in three amino acids, all belonging to groups with strongly similar properties (Supplementary Fig. 1a). The same applies to aDHS; the two homologous proteins have an identity percentage of 91.03%, with most of the differing residues belonging to groups with similar properties (Supplementary Fig. 1a)

Expression and purification of recombinant *S. solfataricus* aIF5A in *E. coli*

The gene coding for *S. solfataricus* aIF5A (ORF Sso0970) was cloned into pMCSG7 expression vector using Ligation Independent Cloning (LIC) as described previously (Aslanidis and de Jong, 1990) and used to transform *E. coli* ROSETTA (DE3)/ pLysS cells. ORF Sso0970 was PCR amplified using primers suitable for LIC cloning, (Forward: 5'-TACTTCCAATCCAATGCCGCATAACGTACACG-3'; Reverse: 5'-TTATCCACTTCCAATGCTTAACCCTAACTATT-3'; underlined regions represent LIC tails). The cloned aIF5A gene produces the full-length initiation factor plus ten histidine residues at the N-terminus, a ten amino acid peptide linker, and the specific cleavage site (ENLYFQ) for the Tobacco Etch Virus (TEV) protease.

One of the positive colonies was inoculated in 2 l of LB medium containing 34 g.ml^{-1} chloramphenicol and 100 g.ml^{-1} ampicillin and grown at 37 °C until an OD600 of 0.7 was reached, at this point the culture was

induced by adding 0.5 mM IPTG. After 4 hours cells were harvested, pelleted and resuspended in 20 ml of lysis buffer (50 mM Tris-HCl pH 7.8, 150 mM NaCl, 15 mM imidazole, 1mM PMSF, 10 $\mu g.mL^{-1}$ DNase I, 25 $\mu g.mL^{-1}$ lysozyme). Cells were disrupted by sonication and the lysate was clarified by centrifugation at 100.000 g for 40 min at 4°C. To allow binding of the His-tagged aIF5A, the supernatant was loaded into a pre-equilibrated PROTINO Ni-NTA column (Macherey-Nagel) installed on a ÄKTA start chromatography system. Washing buffer (50 mM Tris-HCl pH 7.8, 500 mM NaCl, 40 mM imidazole) was used to rinse the lysate and beads until the absorbance signal (A280) reached the baseline. The protein was then eluted in 4 ml of elution buffer (50 mM Tris-HCl pH 7.8; 150 mM NaCl; 250 mM imidazole) and digested with TEV protease to remove the His-tag. TEV protease was added in a 1:50 (TEV/aIF5A) ratio and incubated overnight at 4°C. Therefore, the cleaved protein was purified once more using a PROTINO Ni-NTA column that had excess of TEV and HIS-tag. Purified aIF5A was dialyzed in dialysis buffer (50 mM Tris-HCl pH 7.8, 150 mM NaCl) overnight at 4°C and collected in small aliquots stored at -80°C. SDS-PAGE was used to analyze all of the steps.

Expression and purification of recombinant *S. islandicus* DHS from *E. coli*

The *S. islandicus* aDHS ORF M1627 1306 gene was amplified by PCR using 100 ng genomic DNA and the following primers: forward 5'AAAAGCATGCGCATAAATAGAGAGGACTTGTTAAAAAACCC3' (SphI restriction site) reverse 5'AAAAGGATCCGCTTAATAAAGACGCGGCCAAAATAGG3' (BamHI restriction site). Amplified ORF was cloned in the plasmid pQE-

70 (Quiagen), which gives the recombinant protein a C-terminal His-tag. With the exception of the TEV cleavage, which was not possible to carry out with this expression plasmid, His-tagged aDHS protein was purified using the same procedure as for aIF5A. The purified protein was O.N. dialyzed against DHS dialysis buffer (50 mM Tris HCl pH 8.5, 500 mM NaCl, 80 mM Imidazole, 10% Glycerol).

Isothermal titration calorimetry

ITC measurements were performed at 5°C, 20°C, 25°C and 30°C on a MicroCal PEAQ-ITC (Malvern Panalytical). The ITC buffer was made with 50 mM Tris, HCl pH 8.5, 150 mM NaCl, 50 mM Imidazole, 10% Glycerol. In a typical experiment, 1.5 or 2 µl aliquots of aIF5A at 5 $mg.ml^{-1}$ were injected into a solution of aDHS at 0.5 $mg.ml^{-1}$ in the 200 µl sample cell. The delay between injections was set to 200-300 s. ITC titration curves were analyzed using a single binding site model using AFFINImeter (Piñeiro et al., 2019) and Malvern MicroCal PEAQ-Analysis softwares.

Crystallization, data collection, structure refinement and model prediction

Crystallization was carried out by the vapor diffusion method. Sitting drops were set by mixing one volume of protein solution recovered after ITC analysis (Da Veiga et al., 2016) (7 $mg.ml^{-1}$) with one volume of reservoir solution (200 mM sodium trihydrate acetate pH 8.0, 16% PEG 3350) and equilibrated against reservoir solution incubated at 4°C. Single crystals diffracting anisotropically were obtained, cryoprotected by soaking about 5 min into a cryoprotection solution made with Glycerol

15%, PEG 3350 25%, and then flash-freezed into liquid ethane. Diffraction data were collected on the X06DA beamline at the Swiss Light Source synchrotron in Villigen, Switzerland and processed using XDS (Kabsch, 2010), autoPROC (Vonrhein et al., 2011) and STARANISO (Global Phasing Ltd, Cambridge, United Kingdom. http://staraniso.globalphasing.org/cgi-bin/staraniso.cgi). Initial phases were obtained using molecular replacement with MOLREP (Vagin and Teplyakov, 2010) using a aDHS tetramer model generated with ColabFold as a search model (Mirdita et al., 2022). Four aIF5A molecules were then located and placed using Fourier difference maps (and the AlphaFold2 model as a starting model). Refinement was carried out using the PHENIX package (Afonine et al., 2012) and model were built with Coot (Emsley et al., 2010). Four NAD molecules, copurified with aDHS, were located and placed at a later stage of the refinement based on Fourier difference maps. Although the integrity of the purified aIF5A has been confirmed by SDS-PAGE (Supplementary Fig. 1) and mass spectrometry (Supplementary Fig. 10), the C-terminal domains of all four aIF5A in the asymmetric unit are not visible in the electron density map, not being stabilized by crystal contacts and free to move in solvent channels. As a consequence, they were modeled based on former IF5A structures and AlphaFold2 structure predictions. No density is also visible for the residues 276 to 290 in the four aDHS molecules in the loop connecting bB and bA. We attempted to soak crystals in a stabilization solution containing the spermidine analogue GC7 (N1-guanyl-1,7-diamineoheptane), but without success since no additional density was visible in Fourier difference maps. Coordinates of the aDHS-aIF5A-NAD complex have been deposited in the PDB database (PDB ID 8PUT).

Molecular docking

Docking calculations were performed using the Glide Software included in the Schrödinger suite 2021-4. Initial trials were performed with the standard XP protocol that does not account protein flexibility. However, all this run did not produce any relevant pose. For this reason, Induced Fit Docking (IFD) protocol was applied allowing the flexibility of residues within 5 Å from ligand, using the extended sampling protocol. At the beginning of the calculation, the residues at 5 Å from ligand and the grid center was defined based on the spermidine position in the hDHS structure (PDBID: 6XXJ). The best docking pose, with an IFD score of -61705.30 was selected as the best pose.

Ensemble docking calculation was performed after a cluster analysis of all the chains in all the MD simulations based on the aDHS binding site heavy atoms. The gromos clustering method was used to perform clustering with a cut-off value of 2 Å. The clusters with at least 30 frames (0.1% of all the frames) were selected for the ensemble docking calculations, resulting in a total of 19 clusters. Standard Glide XP docking was performed on all these receptor conformations.

ACKNOWLEDGMENTS

We are extremely grateful to Dr Vincent Oliéric for help during data collection at SLS Viligen (Switzerland), and we would like to thank Dr Karl Brillet and Dr Philippe Benas for help in ITC and DLS experiments on the MoBioFaSt platform. M.D. was recipient of an EMBO short term fellowship. This work was supported by the Centre National de la Recherche Scientifique (CNRS) and by the Cortecs Scientific Core

Facilities of the University of Strasbourg. D.D.M. acknowledges the support of the Italian Foundation for Cancer Research AIRC (Project No. IG 807 2022 ID 27534).

AUTHORS CONTRIBUTIONS

E.E., A.L.T. and A.S. conceptualized and designed the study. A.R. and M.D. constructed the expression vector and set-up the expression protocol. M.D. expressed and purified proteins and performed DLS experiments. E.E. and M.D. performed and analyzed ITC experiments. M.D. and A.S. crystallized the complex. E.E. solved and refined the X-ray structure. M.D., F.S. and A.P. made SAXS measurements. F.S. made SAXS data analysis. S.M. and D.D.M. performed and rationalized computational analysis. P.W. made mass spectrometry experiments. M.D, E.E, SM, made the figures. All authors contributed to writing the manuscript.

COMPETING INTERESTS

The authors declare no competing interests.

REFERENCES

Afonine, P.V., Grosse-Kunstleve, R.W., Echols, N., Headd, J.J., Moriarty, N.W., Mustyakimov, M., Terwilliger, T.C., Urzhumtsev, A., Zwart, P.H., and Adams, P.D. (2012). Towards automated crystallographic structure refinement with *phenix.refine*. Acta Crystallographica Section D Biological Crystallography *68*, 352-367.

Aslanidis, C., and de Jong, P.J. (1990). Ligation-independent cloning of PCR products (LIC-PCR). Nucleic Acids Res. *18*, 6069-6074.

Barba-Aliaga, M., and Alepuz, P. (2022). Role of eIF5A in Mitochondrial Function. International Journal of Molecular Sciences *23*, 1284.

Bassani, F., Romagnoli, A., Cacciamani, T., Amici, A., Benelli, D., Londei, P., Märtens, B., Bläsi, U., and La Teana, A. (2018). Modification of translation factor aIF5A from Sulfolobus solfataricus. Extremophiles *22*, 769-780.

Burnouf, D., Ennifar, E., Guedich, S., Puffer, B., Hoffmann, G., Bec, G., Disdier, F., Baltzinger, M., and Dumas, P. (2012). kinITC: a new method for obtaining joint thermodynamic and kinetic data by isothermal titration calorimetry. J. Am. Chem. Soc. *134*, 559-565.

Da Veiga, C., Mezher, J., Dumas, P., and Ennifar, E. (2016). Isothermal Titration Calorimetry: Assisted Crystallization of RNA–Ligand Complexes. In Nucleic Acid Crystallography, E. Ennifar, ed. (Springer New York), pp. 127-143.

Dever, T.E., Gutierrez, E., and Shin, B.S. (2014). The hypusine-containing translation factor eIF5A. Crit. Rev. Biochem. Mol. Biol. *49*, 413-425.

Emsley, P., Lohkamp, B., Scott, W.G., and Cowtan, K. (2010). Features and development of *Coot*. Acta Crystallographica Section D Biological Crystallography *66*, 486-501.

Ganapathi, M., Padgett, L.R., Yamada, K., Devinsky, O., Willaert, R., Person, R., Au, P.-Y.B., Tagoe, J., McDonald, M., Karlowicz, D., et al. (2019). Recessive Rare Variants in Deoxyhypusine Synthase, an Enzyme Involved in the Synthesis of Hypusine, Are Associated with a Neurodevelopmental Disorder. The American Journal of Human Genetics *104*, 287-298.

Gutierrez, E., Shin, B.-S., Woolstenhulme, Christopher J., Kim, J.-R., Saini, P., Buskirk, Allen R., and Dever, Thomas E. (2013). eIF5A Promotes Translation of Polyproline Motifs. Mol. Cell *51*, 35-45.

Hoque, M., Park, J.Y., Chang, Y.-j., Luchessi, A.D., Cambiaghi, T.D., Shamanna, R., Hanauske-Abel, H.M., Holland, B., Pe'ery, T., Tian, B., and Mathews, M.B. (2017). Regulation of gene expression by translation factor eIF5A: Hypusine-modified eIF5A enhances nonsense-mediated mRNA decay in human cells. Translation *5*, e1366294.

Joe, Y.A., Wolff, E.C., Lee, Y.B., and Park, M.H. (1997). Enzyme-Substrate Intermediate at a Specific Lysine Residue Is Required for Deoxyhypusine Synthesis. J. Biol. Chem. *272*, 32679-32685.

Kabsch, W. (2010). Integration, scaling, space-group assignment and post-refinement. Acta Crystallographica Section D Biological Crystallography *66*, 133-144.

Kulkarni, A., Anderson, C.M., Mirmira, R.G., and Tersey, S.A. (2022). Role of Polyamines and Hypusine in β Cells and Diabetes Pathogenesis. Metabolites *12*, 344.

Lee, C.H., Um, P.Y., and Park, M.H. (2001). Structure–function studies of human deoxyhypusine synthase: identification of amino acid residues critical for the binding of spermidine and NAD. Biochemical Journal *355*, 841-849.

Liao, D.-I., Wolff, E.C., Park, M.H., and Davies, D.R. (1998). Crystal structure of the NAD complex of human deoxyhypusine synthase: an enzyme with a ball-and-chain mechanism for blocking the active site. Structure *6*, 23-35.

Manjunath, H., Zhang, H., Rehfeld, F., Han, J., Chang, T.-C., and Mendell, J.T. (2019). Suppression of Ribosomal Pausing by eIF5A Is Necessary to Maintain the Fidelity of Start Codon Selection. Cell Reports *29*, 3134-3146.e3136.

Mathews, M.B., and Hershey, J.W.B. (2015). The translation factor eIF5A and human cancer. Biochim. Biophys. Acta *1849*, 836-844.

Mirdita, M., Schütze, K., Moriwaki, Y., Heo, L., Ovchinnikov, S., and Steinegger, M. (2022). ColabFold: making protein folding accessible to all. Nat. Methods *19*, 679-682.

Nakanishi, S., and Cleveland, J.L. (2016). Targeting the polyamine-hypusine circuit for the prevention and treatment of cancer. Amino Acids *48*, 2353-2362.

Ning, L., Wang, L., Zhang, H., Jiao, X., and Chen, D. (2020). Eukaryotic translation initiation factor 5A in the pathogenesis of cancers

(Review). Oncology Letters *20*, 1-1.

Park, M.H., and Wolff, E.C. (2018). Hypusine, a polyamine-derived amino acid critical for eukaryotic translation. J. Biol. Chem. *293*, 18710-18718.

Park, M.H., Kar, R.K., Banka, S., Ziegler, A., and Chung, W.K. (2022). Post-translational formation of hypusine in eIF5A: implications in human neurodevelopment. Amino Acids *54*, 485-499.

Pelechano, V., and Alepuz, P. (2017). eIF5A facilitates translation termination globally and promotes the elongation of many non polyproline-specific tripeptide sequences. Nucleic Acids Res. *45*, 7326-7338.

Piñeiro, Á., Muñoz, E., Sabín, J., Costas, M., Bastos, M., Velázquez-Campoy, A., Garrido, P.F., Dumas, P., Ennifar, E., García-Río, L., et al. (2019). AFFINImeter: A software to analyze molecular recognition processes from experimental data. Anal. Biochem. *577*, 117-134.

Romagnoli, A., Moretti, P., D'Agostino, M., Rexha, J., Perta, N., Piccinini, A., Di Marino, D., Spinozzi, F., and La Teana, A. (2022). Structural–Functional Relationship of the Ribonucleolytic Activity of aIF5A from Sulfolobus solfataricus. Biomolecules *12*, 1432.

Schrader, R., Young, C., Kozian, D., Hoffmann, R., and Lottspeich, F. (2006). Temperature-sensitive eIF5A Mutant Accumulates Transcripts Targeted to the Nonsense-mediated Decay Pathway. J. Biol. Chem. *281*, 35336-35346.

Sfakianos, A.P., Raven, R.M., and Willis, A.E. (2022). The pleiotropic roles of eIF5A in cellular life and its therapeutic potential in cancer. Biochem. Soc. Trans. *50*, 1885-1895.

Spolar, R.S., and Record, M.T. (1994). Coupling of Local Folding to Site-Specific Binding of Proteins to DNA. Science *263*, 777-784.

Tauc, M., Cougnon, M., Carcy, R., Melis, N., Hauet, T., Pellerin, L., Blondeau, N., and Pisani, D.F. (2021). The eukaryotic initiation factor 5A (eIF5A1), the molecule, mechanisms and recent insights into the pathophysiological roles. Cell & Bioscience *11*, 219.

Tong, Y., Park, I., Hong, B.-S., Nedyalkova, L., Tempel, W., and Park, H.-W. (2009). Crystal structure of human eIF5A1: Insight into functional similarity of human eIF5A1 and eIF5A2. Proteins: Structure, Function, and Bioinformatics *75*, 1040-1045.

Turpaev, K.T. (2018). Translation Factor eIF5A, Modification with Hypusine and Role in Regulation of Gene Expression. eIF5A as a Target for Pharmacological Interventions. Biochemistry (Moscow) *83*, 863-873.

Umland, T.C., Wolff, E.C., Park, M.H., and Davies, D.R. (2004). A New Crystal Structure of Deoxyhypusine Synthase Reveals the Configuration of the Active Enzyme and of an Enzyme·NAD·Inhibitor Ternary Complex. J. Biol. Chem. *279*, 28697-28705.

Vagin, A., and Teplyakov, A. (2010). Molecular replacement with *MOLREP*. Acta Crystallographica Section D Biological Crystallography

66, 22-25.

Valentini, S.R., Casolari, J.M., Oliveira, C.C., Silver, P.A., and McBride, A.E. (2002). Genetic Interactions of Yeast Eukaryotic Translation Initiation Factor 5A (eIF5A) Reveal Connections to Poly(A)-Binding Protein and Protein Kinase C Signaling. Genetics *160*, 393-405.

Vonrhein, C., Flensburg, C., Keller, P., Sharff, A., Smart, O., Paciorek, W., Womack, T., and Bricogne, G. (2011). Data processing and analysis with the *autoPROC* toolbox. Acta Crystallographica Section D Biological Crystallography *67*, 293-302.

Wagner, S., and Klug, G. (2007). An Archaeal Protein with Homology to the Eukaryotic Translation Initiation Factor 5A Shows Ribonucleolytic Activity. J. Biol. Chem. *282*, 13966-13976.

Wallace, I.M. (2006). M-Coffee: combining multiple sequence alignment methods with T-Coffee. Nucleic Acids Res. *34*, 1692-1699.

Wątor, E., Wilk, P., and Grudnik, P. (2020). Half Way to Hypusine—Structural Basis for Substrate Recognition by Human Deoxyhypusine Synthase. Biomolecules *10*, 522.

Wątor, E., Wilk, P., Biela, A., Rawski, M., Zak, K.M., Steinchen, W., Bange, G., Glatt, S., and Grudnik, P. (2023). Cryo-EM structure of human eIF5A-DHS complex reveals the molecular basis of hypusination-associated neurodegenerative disorders. Nature Communications *14*, 1698.

Wolff, E.C., Folk, J.E., and Park, M.H. (1997). Enzyme-Substrate Intermediate Formation at Lysine 329 of Human Deoxyhypusine Synthase. J. Biol. Chem. *272*, 15865-15871.

Wu, G.-Q., Xu, Y.-M., and Lau, A.T.Y. (2020). Recent insights into eukaryotic translation initiation factors 5A1 and 5A2 and their roles in human health and disease. Cancer Cell International *20*, 142.

Xu, A., Jao, David L.-E., and Chen, Kuang Y. (2004). Identification of mRNA that binds to eukaryotic initiation factor 5A by affinity co-purification and differential display. Biochemical Journal *384*, 585-590.

Zuk, D. (1998). A single amino acid substitution in yeast eIF-5A results in mRNA stabilization. The EMBO Journal *17*, 2914-2925.